Jurnal Asiimetrik: Jurnal Ilmiah Rekayasa Dan Inovasi
Terakreditasi "**Peringkat 3**" berdasarkan SK Dirjendiktiristek, Nomor: 225/E/KPT/2022
Volume 5 Nomor 2 Tahun 2023, Juli 2023, Halaman 231-242
Website : http://journal.univpancasila.ac.id/index.php/asiimetrik/

p-ISSN 2655-1861
e-ISSN 2716-2923

Pengaruh Geometri Berukuran Mikro Dengan Variasi Bentuk Sebagai Kontrol Aliran Pasif di NACA 4415

The Effect of Micro Geometry with Various Forms as Passive Flow Control in NACA 4415

James Julian[1*], Rizki Aldi Anggara[1], Fitri Wahyuni[1] dan Nely Toding Bunga[2]
[1]Mechanical Engineering, Universitas Pembangunan Nasional Veteran Jakarta, Jawa Barat 12450, Indonesia
[2]Program Studi Teknik Mesin, Fakultas Teknik, Universitas Pancasila, Jakarta 12640, Indonesia

Article information:

Received:
28/02/2023
Revised:
31/03/2023
Accepted:
09/04/2023

Abstract

This study investigates the effect of variations in the micro geometry with various forms as passive flow control devices on the aerodynamic capability of the airfoil. Micro-cylinder, micro-slat, and micro-cube are installed close to the leading edge of the NACA 4415 airfoil as a micro geometric variation of passive flow control devices with a predetermined diameter of 3% c located at coordinates x= 0% c and y= 8 %c of the leading edge of the airfoil. The Reynolds number used in this study is Re = 10^6 with AoA variations from 0°-30°. This study's results show a decrease in Cl of 12% with a micro-cylinder, 26% with a micro-slat, and 28% with a micro-cube. In addition, the Cd produced by using the variation of the device micro geometry has increased significantly. Thus, the final result is a lift-to-drag ratio of more petite than the without micro. In the streamlined contour shown when the airfoil is at a high angle of attack, the use of micro geometric variations of passive flow control devices can have an effect that causes reduced recirculation that occurs in the airfoil. However, the impact of these devices is not optimal, resulting in a reduction in the aerodynamic capability of the NACA 4415 airfoil.

***Keywords**: airfoil, aerodynamic, micro-cube, micro-cylinder, micro-slat.*

***SDGs*:**

Abstrak

Penelitian ini menyelidiki pengaruh variasi geometri berukuran mikro dengan variasi bentuk sebagai perangkat kontrol aliran pasif terhadap performa aerodinamis airfoil. Micro-cylinder, micro-slat, dan micro-cube dipasang dekat dengan leading edge airfoil NACA 4415 sebagai variasi geometri berukuran mikro pada perangkat kontrol aliran pasif dengan diameter yang telah ditentukan sebesar 3% c yang terletak pada koordinat x= 0% c dan y = 8 %c dari tepi depan airfoil. Bilangan Reynolds yang digunakan dalam penelitian ini adalah *Re* = 10^6 dengan variasi AoA dari 0°-30°. Hasil penelitian ini menunjukkan penurunan C_l sebesar 12% dengan micro-silinder, 26% dengan micro-slat, dan 28% dengan micro-cube. Selain itu, C_d yang dihasilkan dengan menggunakan variasi geometri perangkat berukuran mikro telah meningkat secara signifikan. Sehingga, menghasilkan rasio lift-to-drag yang lebih kecil dari tanpa mikro. Pada streamlined contour yang ditunjukkan saat airfoil ketika berada pada sudut serang yang tinggi, penggunaan variasi geometri berukuran mikro dari perangkat kontrol aliran pasif dapat memberikan efek yang menyebabkan berkurangnya resirkulasi yang terjadi pada airfoil. Namun, efek dari perangkat tersebut tidak optimal, mengakibatkan penurunan kemampuan aerodinamis dari airfoil NACA 4415.

Kata Kunci: *airfoil*, aerodinamis, *micro-cube*, *micro-cylinder*, *micro-slat*.

*Correspondence Author
email : zames@upnvj.ac.id

1. INTRODUCTION

Various research and development of fluid mechanics application topics have been carried out. Until now, research on this topic is still developing, especially on the aerodynamic capability of airfoils. Aerodynamics is one of the essential aspects for airfoils to achieve work efficiency levels. Airfoils are generally widely applied to the blades of a wind turbine, helicopter blades, wings of aircraft, and others. The air flowing through the airfoil will affect its aerodynamic capability. In addition, the shape of an airfoil is also the main focus, so it determines the aerodynamic ability of the airfoil. Therefore, various studies have been carried out by making innovations to achieve sufficient aerodynamic capability. One of the many innovations developed is the passive flow control device. Adding these devices is expected to enhance the aerodynamic ability of the airfoil. In practice, passive flow control devices generally have a simple geometric shape. In wind turbines, many installations of passive flow control devices have been carried out; for example, the structure of winglets, micro-cylinder, splits (slots), grooves, vortex generators, flaps and gurney flaps, roughness elements, and textured surfaces (Afungchui, Kamoun and Helali, 2014; Aramendia *et al.*, 2018; Bai *et al.*, 2016; Belamadi *et al.*, 2016; Khaled *et al.*, 2019; Liu *et al.*, 2020; Shi *et al.*, 2019). Besides having an affordable price, passive flow control devices do not need external energy and are manageable to install compared to active flow control devices (Julian, Iskandar, Wahyuni, Armansyah, *et al.*, 2022; Moshfeghi, Ramezani and Hur, 2021).

Several studies discuss passive flow control devices. A study uses a combination of leading-edge slat and micro tab installation as passive flow control on the S809 airfoil. The study results indicate that installing leading-edge slats and micro tabs can effectively enhance the aerodynamic capability of the S809 airfoil by restraining flow separation and increasing the lift coefficient. The micro tab position at 0.95c and altitude at 0.03c improve aerodynamic ability (Li, Wang and Wu, 2022). In addition, other studies discuss the effect of augmenting a micro-cylinder close to the leading edge of the horizontal axis wind turbine blade, which is simulated in three dimensions to increase the wind turbine's power output. The Reynolds Average Navier-Stokes (RANS) equation is used in numerical calculations using the k-ω SST turbulence model. The research was conducted with variations in diameter and location. The study results indicate that installing a micro-cylinder on a wind turbine can increase the wind turbine's power output. The wind turbine's outcome power rises as the micro-cylinder's diameter decreases. At the micro-cylinder location, it was found that the power output increased for all variations.

In addition, placing the micro-cylinder on the pressure side will have a more negligible effect on the wind turbine's power output than placing it close to the leading edge of the turbine blades (Mostafa *et al.*, 2022). Furthermore, other studies are investigating passive flow control devices to enhance the capability of bidirectional Horizontal-axis tidal turbines (BHATT). Various passive flow control devices, such as fences, winglets, and squealers, are used. This research was conducted with a 3-dimensional model using k-ω SST as a turbulence model. The results of this study indicate that wing fences suppress spanwise flow over the suction surface, although they do not enhance BHATT capability. The centrosymmetric winglet circuit is designed and optimized to inhibit wingtip vortices that form and increase rotor torque. Thus, the optimal BHATT can produce 2.3% additional energy at the design tip strip ratio (TSR) (Zhang *et al.*, 2022).

Based on the research that has been done on passive flow control devices, it is proven that the installation of these devices can enhance the aerodynamic capability of the airfoil. Various highlights from research on passive flow control devices are described in Table 1. Table 1 shows that this study has an update regarding the discussion of passive flow control devices. Passive flow control devices are sensitive to the shape and size of the geometry. Therefore, a deeper study of passive flow control devices is needed. This research was conducted with various geometric shapes on passive flow control devices. The variations used are micro-cylinder, slat, and micro cube, installed close to the airfoil's leading edge.

Table 1. Several Studies about passive flow control

Study	Slat	Micro-cylinder	Micro-slat	Bluff-body	Microtab	Wing fence	Cavity
Li, Wang and Wu, 2022	Yes	No	No	No	Yes	No	No
Mostafa *et al.*, 2022	No	Yes	No	No	No	No	No
Zhang *et al.*, 2022	No	No	No	No	No	Yes	No
Julian *et al.*, 2023	No	No	No	No	No	No	Yes
Julian *et al.*, 2022	Yes	No	No	No	No	No	No
Current study	No	Yes	Yes	Yes	No	No	No

Based on the geometry variation used, each geometric shape represents different flow characteristics as a passive flow control device. On devices with slat geometry, this is the general shape of the airfoil. In general, the airfoil represents the aerodynamic geometry characteristics of a streamlined body. Therefore, the slat is expected to be capable of directing fluid flow to fill the recirculation area. Devices with cylindrical geometric shapes have different flow characteristics as passive flow control. Because of its curved shape, the cylindrical geometry is expected to control fluid flow through the Coanda effect at a certain Reynolds number. Whereas the geometry of the cube-shaped device, it is a geometry that represents the basic shape of the bluff body, which has the characteristics to produce flow separation. Thus, the device with a cube shape is expected to be able to break down the recirculation area, whose role is as a passive flow control device. Based on the three geometric shapes of passive flow control devices, this study aims to examine the influence of the geometric variation of the passive flow control device on the aerodynamic capability of the NACA 4415 airfoil.

2. METHODOLOGY

2.1. NACA 4415

The NACA series airfoil was created and developed by the National Advisory Committee for Aerodynamics (NACA) (Iskandar and Julian, 2022; Julian, Iskandar, Wahyuni, Ferdyanto, *et al.*, 2022; H. Harinaldi *et al.*, 2019; Megawanto *et al.*, 2018; Rubel *et al.*, 2016). NACA 4415 airfoil was chosen as the object to be investigated in this study. NACA series airfoils are very diverse and are represented in the form of numeric digits. Digits represent the shape of the airfoil used. The first digit indicates that the maximum space in the airfoil is 4% of the chord length. Besides that, the second digit represents the chamber position, which is 40% of the note length. The last two digits denote that the maximum airfoil thickness is 15% of the chord length. NACA 4415 airfoil can be seen in Figure 1.

Figure 1. NACA 4415

2.2. Governing Equation and Turbulence Model

This study uses the Reynolds Averaged Navier-Stokes (RANS) equation as the basis for numerical calculations using computational methods. This equation is generally used in CFD applications with numerical methods. The RANS equation can be seen in equations 1 and 2 (Aftab *et al.*, 2016; Harinaldi *et al.*, 2019, 2016; Julian *et al.*, 2016, 2018; Harinaldi *et al.*, 2020; Karim and Julian, 2018; Julian, Iskandar, Wahyuni and Ferdyanto, 2022; Julian *et al.*, 2017). Equation 1 represents the continuity equation of the fluid flow. While equation 2 represents the momentum flow equation. The turbulent model used in this study is k-ε. The k-ε model is a simple turbulence model. In addition, this turbulence model is commonly used in computational methods because it has good resistance, is affordable, and has good accuracy. The k-ε turbulence model is a semi-empirical model built on the transport equation model for the kinetic energy of k turbulence and the dissipation rate (Ahsan, 2014; Julian *et al.*, 2016).

The k-ε turbulence model can be seen in equations 3 and 4.

$$\frac{\partial \rho}{\partial t} + \frac{\partial}{\partial x_i}(\rho u_i) = 0 \quad (1)$$

$$\frac{\partial}{\partial t}(\rho u_i) + \frac{\partial}{\partial x_i}(\rho u_i u_j) = \frac{\partial \rho}{\partial x_i} + \frac{\partial}{\partial x_j}\left[\mu\left(\frac{\partial u_i}{\partial x_j} + \frac{\partial u_j}{\partial x_i} - \frac{2}{3}\delta_{ij}\frac{\partial u_i}{\partial x_j}\right)\right] + \frac{\partial}{\partial x_i}(\rho\overline{u'_i u'_j}) \quad (2)$$

$$\frac{D}{Dt}(\rho k) = \frac{\partial}{\partial x_j}\left[\left(\mu + \frac{\mu_t}{\sigma_k}\right)\frac{\partial k}{\partial x_j}\right] + G_k - \rho\varepsilon \quad (3)$$

$$\frac{D}{Dt}(\rho\varepsilon) = \frac{\partial}{\partial x_j}\left[\left(\mu + \frac{\mu_t}{\sigma_{\varepsilon 2}}\right)\frac{\partial \varepsilon}{\partial x_j}\right] + C_{el}\frac{\varepsilon}{k}G_k - \rho C_{\varepsilon 2}\frac{\varepsilon}{k} \quad (4)$$

2.3. Geometries Detail

This study investigates the effect of variations in the geometric shape of a passive flow control device on the capability of the NACA 4415 airfoil. The geometric shapes of the passive flow control devices used represent the characteristics of each flow. This study covers three types of geometry: the streamlined body, the cylinder body, and the basic geometry of the bluff body. The first model simulates the NACA 4415 airfoil without passive flow control devices. The second model simulates a micro-cylinder installed close to the leading edge of the NACA 4415 airfoil. In the third model, a NACA 6441 airfoil-shaped micro-slat is installed close to the leading edge of the NACA 4415 airfoil. The fourth model simulates a micro-cube-shaped geometry installed close to the leading-edge airfoil NACA 4415. The three geometry variations installed are micro-sized, namely 3% c. In addition, it is placed in the exact location at coordinates y = 8% c. The four simulation models are placed in the fluid domain, shaped by a combination of semicircles and squares. Details of the size of the simulation model and the fluid domain can be seen in Figure 2.

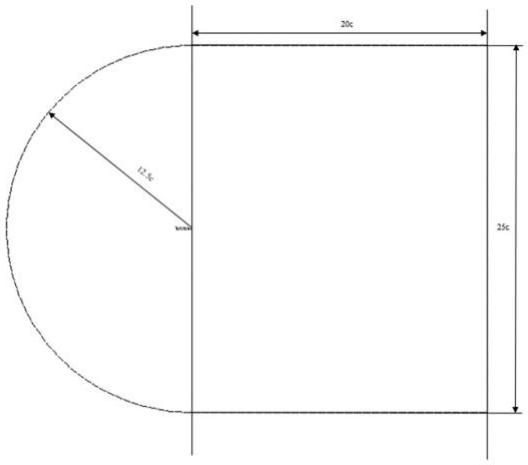

(a). Fluid domain

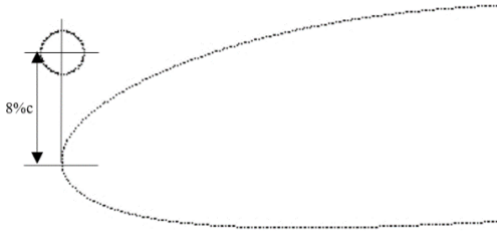

(b). Airfoil with micro-cylinder

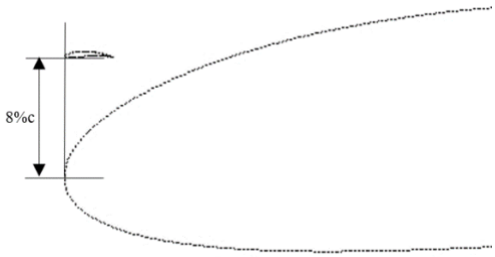

(c). Airfoil with micro-slat

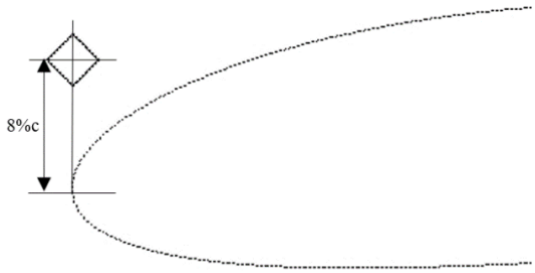

(d). Airfoil with micro-cube

Figure 2. Model simulation

2.4. Meshing and Boundary Condition

In this study, the unstructured mesh with triangular mesh elements with the Reynolds number is Re =10^6. The location of the passive flow control geometries is determined based on the (x,y) coordinates with the NACA 4415 leading edge airfoil as the center point. The fluid domain of this study is divided into two conditions, namely velocity-inlet with a velocity magnitude of 14.77 m/s and zero pressure outlet. Boundary conditions on the airfoil and three geometric shapes of passive flow control devices are defined as a wall (no slip). Details of the mesh and boundary conditions can be seen in Figure 3. In addition, the boundary condition parameters used in this study can be seen in Table 2.

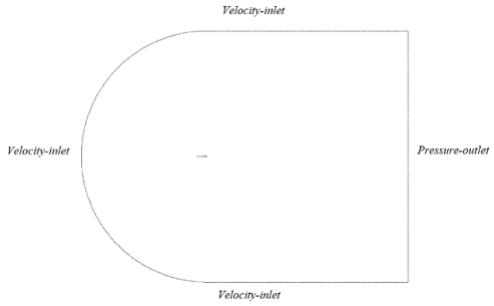

Figure 3. Detail mesh and boundary condition

Table 2. Boundary condition parameters

Parameters	Values
Reynold number (*Re*)	10^6
Inlet	14.77 m/s
Outlet	0 Pa

2.5. Mesh Independence Test

The mesh independence test is performed to determine which mesh has a minor error value to ensure the accuracy of the mesh used in this study. Three variations have been selected. The first variation is a fine mesh with a total of 202368 mesh. The second variation is medium mesh with a capacity of 162768 mesh. In contrast, the third variation is the coarse mesh with a total of 130277. The variation of the mesh can be seen in Figure 4.

In the mesh independence test process, the method used is based on Richardson's extrapolation, which is generalized by Roache (Jacobs and Sherman, 1937). Fluid flow velocity at x= 0.5 and y=0.15 are used as a sample used in this mesh independence test. The first step in the mesh independence test is to define the ratio of grid variations using equation 5. The next step is to determine the order value using equation 6. After selecting the order value in this study, the third step is to determine the error value of the grid using the Grid Convergence Index (GCI). This paper uses two GCIs calculated by equations 7 and 8. The first GCIs is GCIfine, the error value between the fine and medium mesh. While the second GCIs is GCIcoarse, defined as the value of error between the medium and coarse mesh. After determining the GCI, the GCI is investigated using equation 9 to show the variation of the mesh used in the convergence area. If the interpretation of mesh convergence is, the last step can be done with equation 10 as a parameter value to determine the error value for each mesh. Based on the calculation results, the mesh value that has the smallest error value is the fine mesh with a total of 202368 mesh. So, this research will be continued using a fine mesh.

The results of the mesh independence test can be seen in Table 3.

$$r = \frac{h_2}{h_1} \tag{5}$$

$$\bar{\bar{p}} = \frac{l\,n\left(\frac{f_3 - f_2}{f_2 - f_1}\right)}{l\,n(r)} \tag{6}$$

$$GCI_{fine} = \frac{F_s|\epsilon|}{(r^{\bar{\bar{p}}} - 1)} \tag{7}$$

$$GCI_{coarse} = \frac{F_s|\epsilon| r^{\bar{\bar{p}}}}{(r^{\bar{\bar{p}}} - 1)} \tag{8}$$

$$\frac{GCI_{coarse}}{GCI_{fine} r^{\bar{\bar{p}}}} \approx 1 \tag{9}$$

$$f\,r_{h=0} = f_1 + \frac{((f_1 - f_2))}{(r^{\bar{\bar{p}}} - 1)} \tag{10}$$

Table 3. Grid independency study result

Mesh	Fine	Medium	Coarse
Velocity	16.2648	16.301	16.3995
$\bar{\bar{p}}$		4.485890018	
r		1.25	
GCI_{fine}		0.161%	
GCI_{coarse}		0.4389%	
$f_{rh} = 0$		16.24376565	
$\frac{GCI_{coarse}}{GCI_{fine} r^{\bar{\bar{p}}}}$		1.00187	
Error	0.12949%	0.35235%	0.95873%

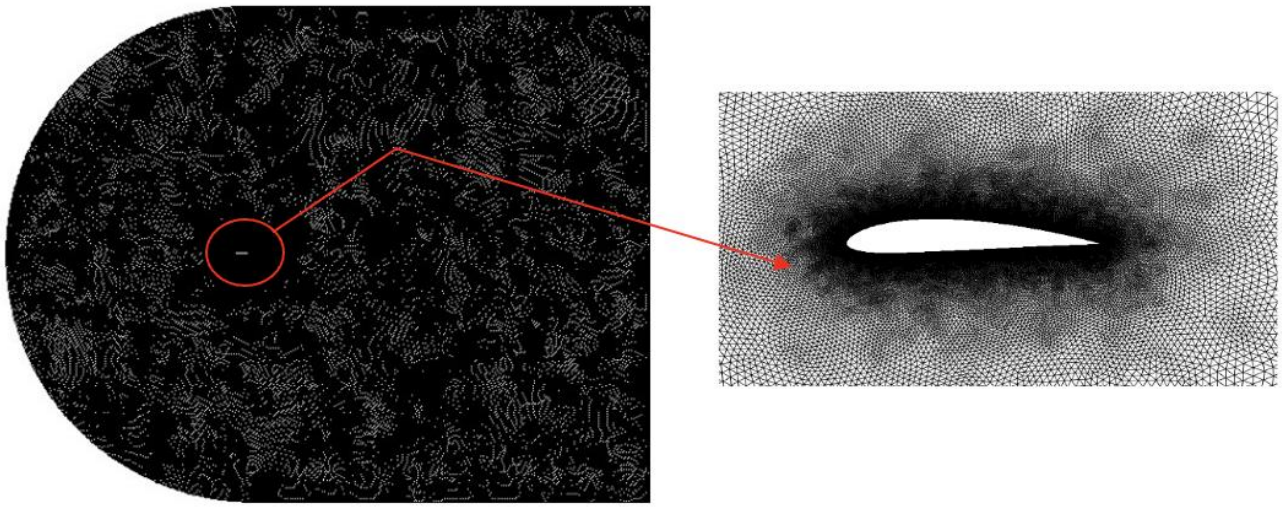

(a). Fine

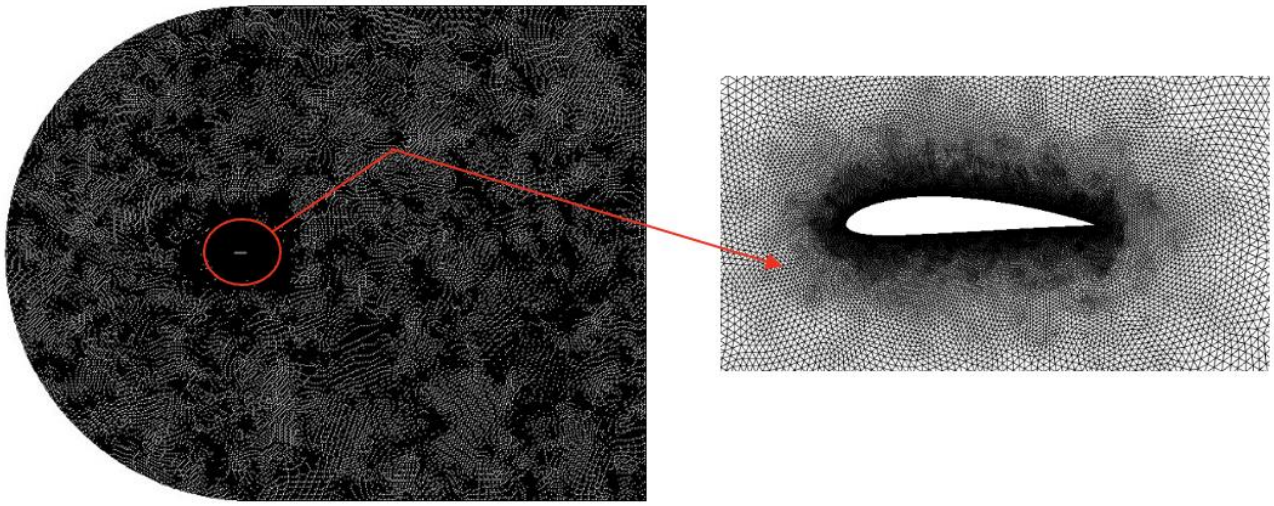

(b). Medium

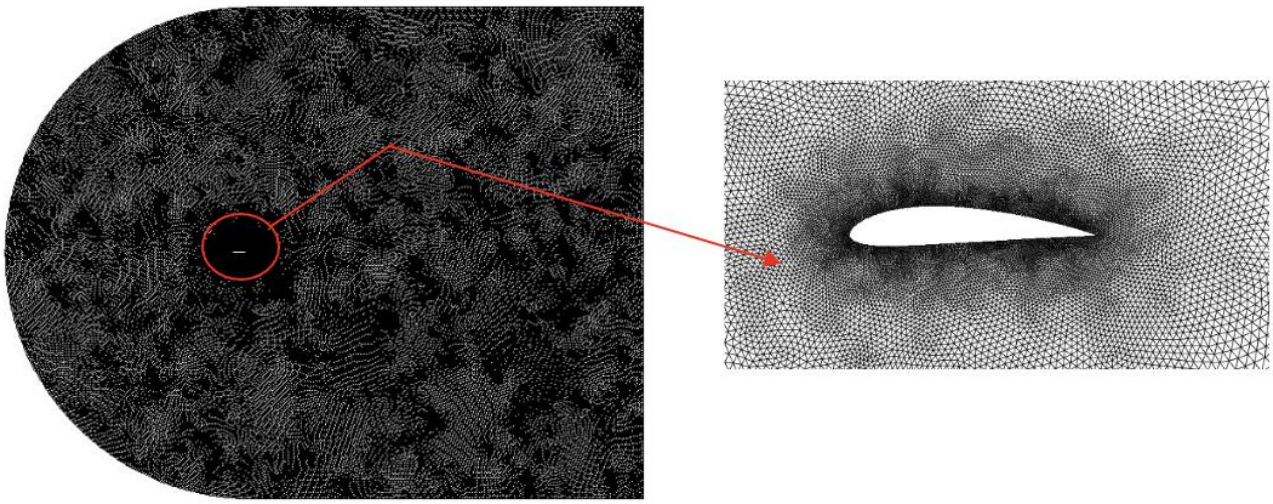

(c). Coarse

Figure 4. Variations of mesh

3. RESULTS AND DISCUSSION

In this study, the data obtained must be validated before data analysis. Validation is carried out to ensure that the studied model meets the actual fluid flow conditions. The computational results obtained in this study were compared with experimental data research conducted by Hoffman (Hoffmann, Reuss Ramsay and Gregorek, 1996).

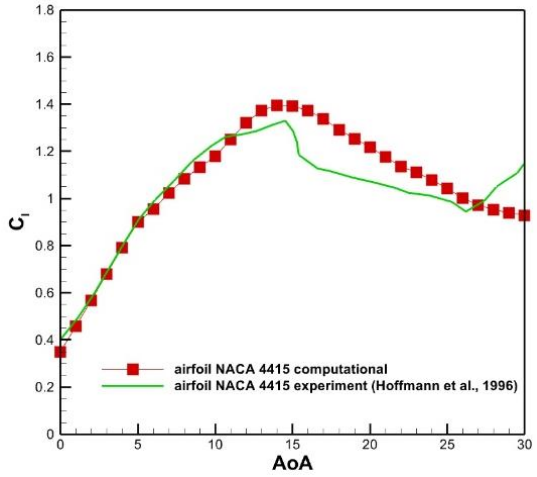

(a). Graph of C_l against changes AoA

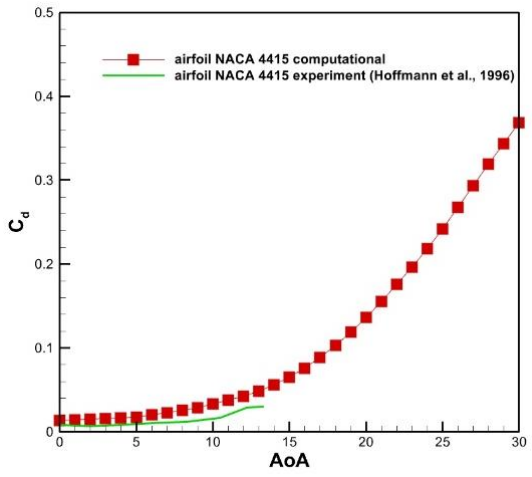

(b). Graph of C_d against changes AoA

Figure 5. Validation C_l and C_d

Airfoil NACA 4415 without passive flow control devices with Reynolds number of $Re = 10^6$ was used as a validation sample. The data compared between the computational and experimental data are Cl and Cd, as shown in Figure 5. In Figure 5a, there is a slight difference in Cl in the computational data with the experimental data. The difference begins when the NACA 4415 airfoil has passed the AoA of 11°. However, the two data show no difference in the airfoil stall phenomenon. The computational and experimental data show that the data stall occurs after an AoA of 14°. Overall, the Cl curve shown in the computational data has a corresponding trend in the experimental data. In the Cd validation, Figure 5b shows that the computational and experimental data curves are very similar and show the same direction. The more significant the AoA, the greater the increase in Cd. Thus, both Cl and Cd data indicate that the computational results are valid.

Passive flow control devices can influence fluid flow through the airfoil. The three geometric variations of passive flow control devices are installed close to the leading edge of the NACA 4415 airfoil with coordinates y=8% with a diameter of 3%c. These geometric variations are expected to affect the aerodynamic capability of the NACA 4415 airfoil.

Figure 6 shows the results of the computations regarding the effect of the installation of geometric variations of passive flow control devices on the aerodynamic capability of the airfoil based on Cl, Cd, and CM data. In Figure 6a, the Cl curve in each sample has a difference. Installing geometric variations of passive flow control devices close to the leading edge of the NACA 4415 airfoil causes a decrease in aerodynamic capability, which is indicated by a reduction in the Cl curve. Based on the Cl curve shown in the installation of micro-slat and micro-cube has a similar trend. In addition, the stall event on installing the micro-slat and micro-cube occurred faster, at AoA=14°.

Meanwhile, the NACA 4415 airfoil stall without passive flow control devices occurred at AoA=15°. The two devices did not have a good effect on the NACA 4415 airfoil. However, there are differences in the results obtained in installing the micro-cylinder. Although there is a decrease in the Cl curve in the airfoil with a micro-cylinder, this device can delay the stall in the airfoil at AoA= 18°. In addition, the post-stall event also occurred in the installation of this device. Post stall is indicated by an increase in the Cl curve

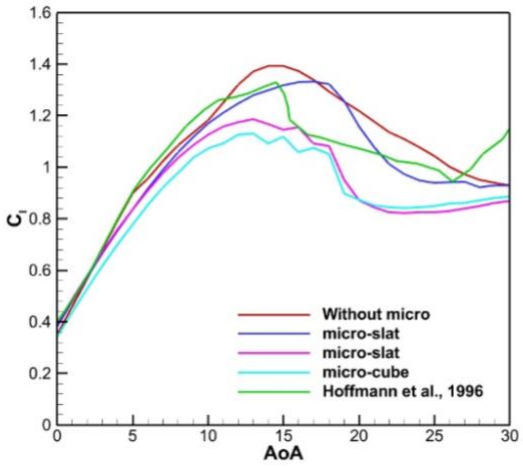

(a). Graph of C_l against changes AoA

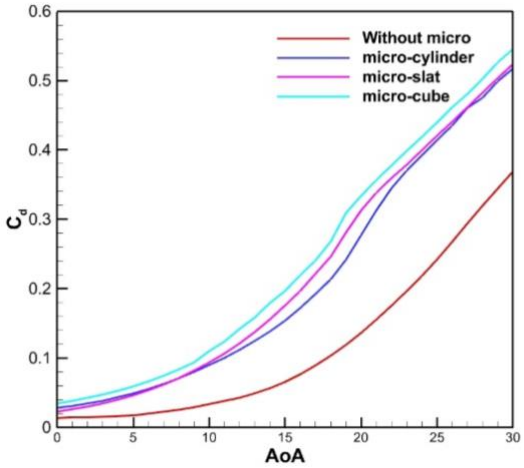

(b). Graph of C_d against changes AoA

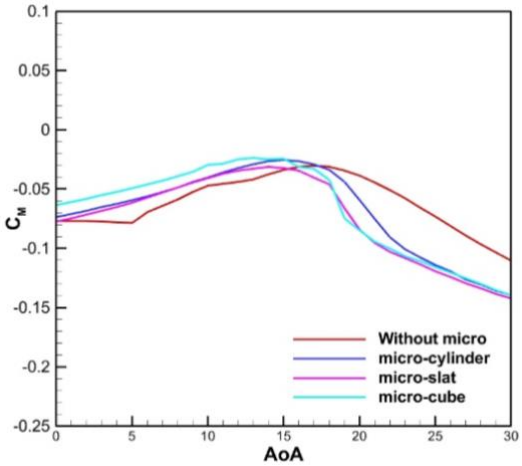

(c). Graph of C_M against changes AoA

Figure 6. Aerodynamic capability of airfoil with and without using flow control devices

after the airfoil stalls. Post-stall on an airfoil with micro-cylinder installation occurs when the airfoil passes AoA = 26˚. In Figure 6b, the decrease in the Cl curve in the structure of passive flow control devices is caused by a significant increase in Cd. The cd will continue to increase as AoA increases. That is caused by flow separation, which causes a flow vacuum in the area on the airfoil's trailing edge so that the drag will arise in the area.

In addition, C_M data is also presented in conducting data analysis, as shown in Figure 6c. The point at 25%c from the leading edge is the aerodynamic center. C_M is a dimensionless parameter that describes the magnitude of the torque value to the total force acting on the phenomenon. C_M affects the level of airfoil stability, where an airfoil is considered stable when a moment equals zero. The resulting C_M curve may be harmful. A negative value on the C_M curve indicates the tendency of the airfoil to experience a torque rotation counterclockwise (pitch down).

Conversely, if the resulting C_M is positive, the torque generated tends to rotate clockwise (pitch up). In Figure 6c, the installation of passive flow control devices affects C_M at every change in AoA. Based on the curve shown, the similarity occurs in the AoA range from 0˚-17˚. After the airfoil has passed AoA by 17˚, the difference in the angle starts to appear. Even though at the AoA, the CM decreased significantly in all samples, the curve shown in the airfoil without passive flow control was more sloping. Thus, Figure 6c shows that installing geometric variations of micro-sized passive flow control devices harms airfoil stability.

In this study, the calculation of the ratio between C_l and C_d was carried out. The lift-to-

drag analysis is carried out to determine which sample has the best aerodynamic capability. The lift-to-drag ratio can be seen in Figure 7. Figure 7 shows that based on the lift-to-drag ratio, the aerodynamic capability of the NACA 4415 airfoil with the installation of passive flow control devices shows unsatisfactory results. Capability declines are sorted from installing the micro-cylinder, followed by the micro-slat to the micro-cube. The smaller the resulting ratio, the greater the ability of the airfoil to produce C_d than to produce C_l.

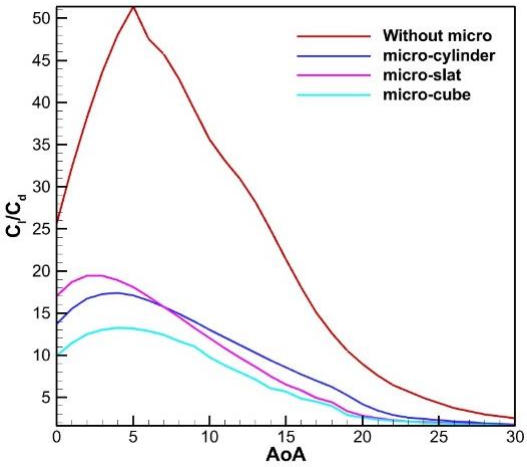

Figure 7. Graph C_l/C_d against changes AoA

The pressure coefficient is also displayed to determine the pressure distribution in the NACA 4415 airfoil. Figure 8 shows the pressure distribution to change in position on the chord length of the airfoil. Pressure distribution is one parameter that determines how well the airfoil performs. In general, airfoils are designed to produce as much pressure on the upper side as possible than on the lower side of the airfoil. This phenomenon aims to enhance the ability of the airfoil to produce good lift. Based on Figure 8, the lower-side airfoil does not show a significant difference between the installation of passive flow control devices and the airfoil without installation. However, there is a big difference on the airfoil's upper side.

A significant pressure drop occurs on the upper side of the airfoil around the leading edge in the installation of passive flow control devices. However, the pressure distribution increases again through the leading-edge area. That adversely affects the airfoil's ability to generate lift. Therefore, a comparison of the area of both the upper-side airfoil and lower-side airfoil is carried out. The large area produced is a parameter of the aerodynamic capability of the airfoil. Because there is no significant difference in the lower side of the airfoil, the area on the upper side of the airfoil has been reviewed. It can be seen in Table 4 that the area produced by the airfoil with the installation of geometric variations of passive flow control devices is lower than the airfoil without micro. The smallest area is obtained by airfoil with micro-cube, followed by micro-slat to micro-cylinder. That is what causes a decrease in the capability of the airfoil.

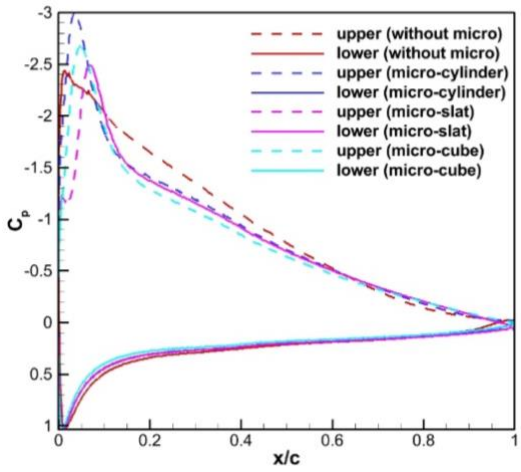

Figure 8. Graph of Cp against changes x/c

Table 4. Area under the curve of Cp

Area	Upper	Lower	Total
Without micro	0.90441	0.25952	1.16393
Micro-cylinder	08577	0.2486	1.1063
Micro-slat	0.79964	0.25131	1.05095
Micro-cube	0.79029	0.22653	1.01682

Furthermore, visualization in the form of contours is carried out to provide a deeper understanding of the role of geometric variations of passive flow control devices on the capability of the NACA 4415 airfoil. The magnitudes of velocity, straight line, and pressure contours are shown in Figure 9 when the airfoil is at AoA 20°. This condition indicates that the airfoil has stalled due to fluid flow recirculation on the upper side of the airfoil, as shown in Figure 9b. So, it will be clear how the influence is given to the geometric

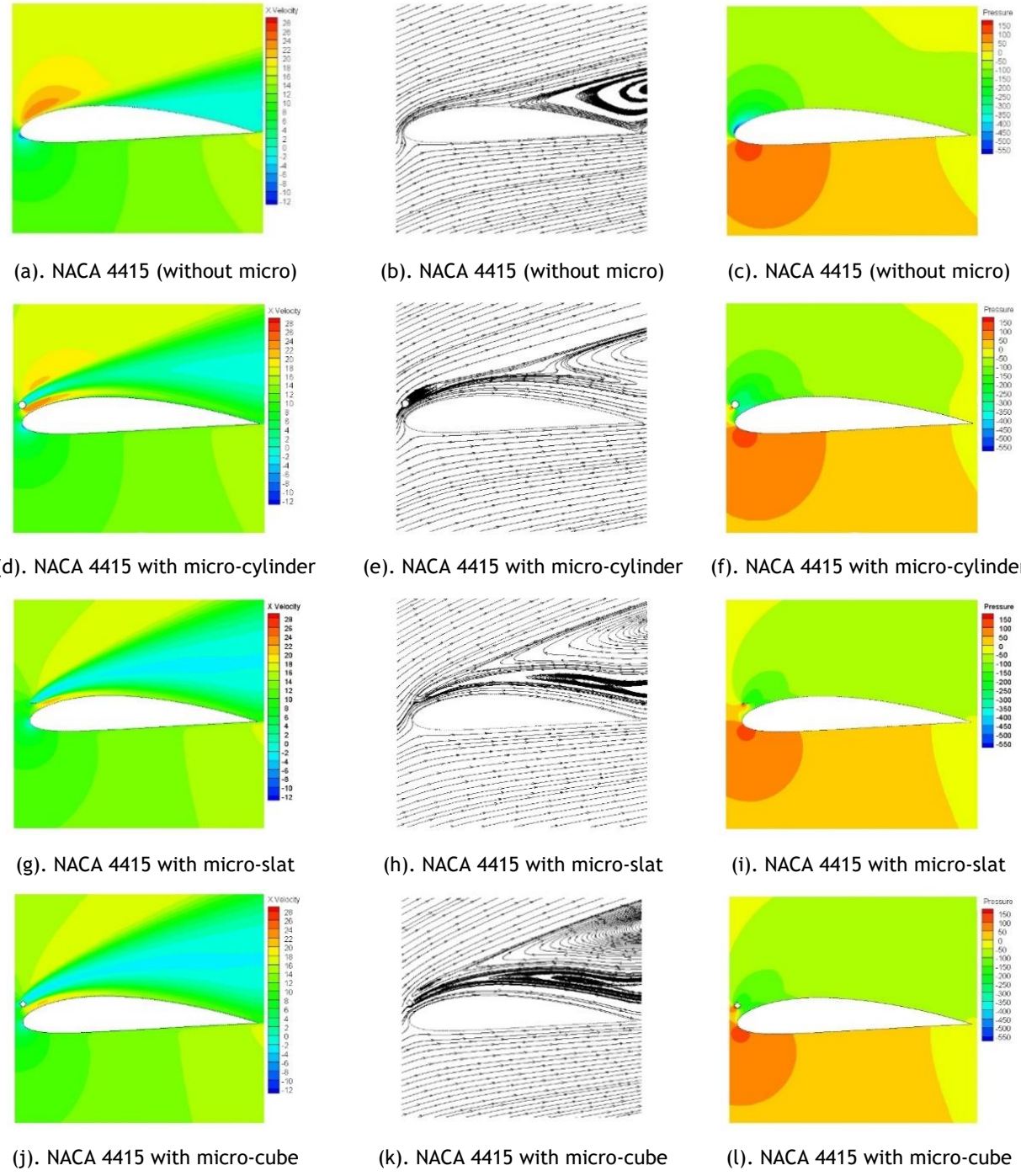

(a). NACA 4415 (without micro) (b). NACA 4415 (without micro) (c). NACA 4415 (without micro)

(d). NACA 4415 with micro-cylinder (e). NACA 4415 with micro-cylinder (f). NACA 4415 with micro-cylinder

(g). NACA 4415 with micro-slat (h). NACA 4415 with micro-slat (i). NACA 4415 with micro-slat

(j). NACA 4415 with micro-cube (k). NACA 4415 with micro-cube (l). NACA 4415 with micro-cube

Figure 9. Magnitude velocity, streamlines contour, and pressure contour at AoA=20°

variation of passive flow control devices on the aerodynamic capability of the airfoil.

Based on the contours shown in Figure 9. Geometric variations of passive flow control can reduce flow recirculation in the airfoil. This ability is seen in the fluid flow that can flow well through the upper side of the airfoil. In general, reducing recirculation is an advantage in improving the aerodynamic capability of the airfoil. When viewed from the angle of C_l and C_d, various passive flow control devices cannot significantly enhance the aerodynamic ability of the NACA 4415 airfoil. Therefore, further research is needed to develop more optimal passive flow control devices.

4. CONCLUSION

This research focuses on the effect of variations in the micro geometry of passive flow control devices on the aerodynamic capability of the NACA 4415 airfoil. Based on the geometric shape of the device, this study uses three variations of micro geometry, namely, micro-cylinder, micro slat, and micro cube. The three variations are installed close to the leading edge of the NACA 4415 airfoil at coordinates y=8%c with a diameter of 3%c. This study uses the Reynolds number of Re = 10^6. Based on the results of this study, the installation of geometric variations of passive flow control devices influences the aerodynamic capability of the NACA 4415 airfoil. However, based on the gradient level of the Cl curve on the installation of micro-cylinder, micro-slat, and micro cube, there was a decrease in Cl of 12%, 26%, and 28%, respectively. In addition, a more significant increase in CD occurred in the installation of geometric variations of passive flow control devices.

In installing micro-slat and micro-cube, stall events occur 1° faster or more precisely at AoA=14°. The micro-cylinder installation can delay the stall by 3° or, more precisely, at AoA=18°. In addition, the post-stall event also occurs when the airfoil with micro-cylinder has passed AoA= 26°. The installation of geometric variations of passive flow control devices also reduces the level of stability of the airfoil, which affects its aerodynamic capability of the airfoil. Based on the lift-to-drag ratio and pressure distribution, there is a decrease in the aerodynamic capability of the airfoil. The installation of these three devices resulted in a decrease in the lift-to-drag ratio. The increasing pressure distribution on the upper side of the airfoil causes this phenomenon. Thus the ability of the airfoil to produce lift is reduced. Therefore, the installation of geometric variations of passive flow control devices does not have the maximum effect on the aerodynamic capability of the NACA 4415 airfoil, even though the installation of geometric variations of passive flow control devices can suppress recirculation in fluid flow.

REFERENCES

Aftab, S.M.A. *et al.* (2016) 'Turbulence Model Selection for Low Reynolds Number Flows', *PLOS ONE*, 11(4), pp. e0153755–e0153770.

Afungchui, D., Kamoun, B. and Helali, A. (2014) 'Vortical structures in the wake of the savonius wind turbine by the discrete vortex method', *Renewable Energy*, 69, pp. 174–179.

Ahsan, M. (2014) 'Numerical analysis of friction factor for a fully developed turbulent flow using k-ε turbulence model with enhanced wall treatment', *Beni-Suef University Journal of Basic and Applied Sciences*, 3(4), pp. 269–277.

Aramendia, I. *et al.* (2018) 'Gurney Flap Implementation on a DU91W250 Airfoil', in *IRCSEEME 2018. The 2nd International Research Conference on Sustainable Energy, Engineering, Materials and Environment*, Spain: MDPI (23), pp. 1448–1453.

Bai, Q. *et al.* (2016) 'Drag reduction characteristics and flow field analysis of textured surface', *Friction*, 4(2), pp. 165–175.

Belamadi, R. *et al.* (2016) 'Aerodynamic performance analysis of slotted airfoils for application to wind turbine blades', *Journal of Wind Engineering and Industrial Aerodynamics*, 151, pp. 79–99.

Harinaldi *et al.* (2019) 'The comparison of an analytical, experimental, and simulation approach for the average induced velocity of a dielectric barrier discharge (DBD)', in *IMAT 2018. The 10th International Meeting Of Advances In Thermofluids (IMAT 2018): Smart City: Advances in Thermofluid Technology in Tropical Urban Development*, Indonesia: AIP Conference Proceedings, p. 020027.

Harinaldi *et al.* (2020) 'Flow Control with Multi-DBD Plasma Actuator on a Delta Wing', *EVERGREEN*, 7(4), pp. 602–608.

Harinaldi, H. *et al.* (2016) 'The effect of plasma actuator on the depreciation of the aerodynamic drag on box model', in *Proceedings Of The 3rd Aun/Seed-Net Regional Conference On Energy Engineering And The 7th International Conference On Thermofluids (RCENE/THERMOFLUID 2015). The 3rd Aun/Seed-Net Regional Conference On Energy Engineering And The 7th International Conference On Thermofluids*, Indonesia: AIP Conference Proceedings, p. 040004.

Harinaldi, H. *et al.* (2019) 'Flow Separation Delay on NACA 4415 Airfoil Using Plasma Actuator Effect', *International Review of Aerospace Engineering (IREASE)*, 12(4), pp. 180–186.

Hoffmann, M.J., Reuss Ramsay, R. and Gregorek, G.M. (1996) *Effects of grit roughness and pitch oscillations on the NACA 4415 airfoil*. NREL/TP-442-7815. National Renewable Energy Lab. (NREL), Golden, CO (United States); The Ohio State Univ., Columbus, OH (United States).

Iskandar, W. and Julian, J. (2022) 'Study of Airfoil Characteristics on NACA 4415 with Reynolds Number Variations', *International Review On Modelling And Simulations (IREMOS)*, 15(3), pp. 162–171.

Jacobs, E.N. and Sherman, A. (1937) *Airfoil Section Characteristics as Affected by Variations of the Reynolds Number*. Other 19930091662. USA: National Advisory Committee for Aeronautics (NACA) and NASA.

Julian, J. *et al.* (2016) 'The Effect of Plasma Actuator Placement on Drag Coefficient Reduction of Ahmed Body as an Aerodynamic Model', *International Journal of Technology*, 7(2), p. 306-313.

Julian, J. *et al.* (2017) 'Review: Flow Control on a Squareback Model', *International Review of Aerospace Engineering (IREASE)*, 10(4), pp. 230–239.

Julian, J. *et al.* (2018) 'Effect of plasma actuator in boundary layer on flat plate model with turbulent promoter', in *Proceedings of the Institution of Mechanical Engineers, Part G: Journal of Aerospace Engineering. The Institution of Mechanical Engineers*, Sage Journals, pp. 3001–3010.

Julian, J., Iskandar, W., Wahyuni, F., Ferdyanto, F., *et al.* (2022) 'Characterization of the Co-Flow Jet Effect as One of the Flow Control Devices', *Jurnal Asiimetrik: Jurnal Ilmiah Rekayasa Dan Inovasi*, 4(2), pp. 185–192.

Julian, J., Iskandar, W., Wahyuni, F. and Ferdyanto, F. (2022) 'Computational Fluid Dynamics Analysis Based On The Fluid Flow Separation Point On The Upper Side Of The NACA 0015 Airfoil With The Coefficient Of Friction', *Media Mesin: Majalah Teknik Mesin*, 23(2), pp. 70–82.

Julian, J., Iskandar, W., Wahyuni, F., Armansyah, A., *et al.* (2022) 'Effect of Single Slat and Double Slat on Aerodynamic Performance of NACA 4415', *International Journal of Marine Engineering Innovation and Research*, 7(2), pp. 93-100.

Julian, J. *et al.* (2023) 'Aerodynamic Performance Improvement on NACA 4415 Airfoil by Using Cavity', *Jurnal Asiimetrik: Jurnal Ilmiah Rekayasa Dan Inovasi*, 5(1), pp. 135–142.

Karim, R.F. and Julian, J. (2018) 'Drag reduction due to recirculating bubble control using plasma actuator on a squareback model', in *ICET4SD 2017. The 2nd International Conference on Engineering and Technology for Sustainable Development*, Indonesia: MATEC Web of Conferences, p. 01108.

Khaled, M. *et al.* (2019) 'Investigation of a small Horizontal-Axis wind turbine performance with and without winglet', *Energy*, 187, p. 115921.

Li, Y., Wang, H. and Wu, Z. (2022) 'Aerodynamic characteristic of wind turbine with the leading edge slat and Microtab', *Sustainable Energy Technologies and Assessments*, 52, p. 101957.

Liu, Y. *et al.* (2020) 'Numerical study of the effect of surface grooves on the aerodynamic performance of a NACA 4415 airfoil for small wind turbines', *Journal of Wind Engineering and Industrial Aerodynamics*, 206, p. 104263.

Megawanto, F.C. *et al.* (2018) 'Numerical analysis of plasma actuator for drag reduction and lift enhancement on NACA 4415 airfoil', in *Proceedings Of The 9th International Conference On Thermofluids 2017 (THERMOFLUID 2017). The 9th International Conference On Thermofluids 2017*, Indonesia: AIP Conference Proceedings, p. 050001.

Moshfeghi, M., Ramezani, M. and Hur, N. (2021) 'Design and aerodynamic performance analysis of a finite span double-split S809 configuration for passive flow control in wind turbines and comparison with single-split geometries', *Journal of Wind Engineering and Industrial Aerodynamics*, 214, p. 104654.

Mostafa, W. *et al.* (2022) 'Quantitative impact of a micro-cylinder as a passive flow control on a horizontal axis wind turbine performance', *Energy*, 244, p. 122654.

Rubel, R.I. *et al.* (2016) 'Comparison of Aerodynamics Characteristics of NACA 0015 & NACA 4415'. Switzerland: Preprints MDPI.

Shi, X. *et al.* (2019) 'Passive flow control of a stalled airfoil using an oscillating micro-cylinder', *Computers & Fluids*, 178, pp. 152–165.

Zhang, J. *et al.* (2022) 'Performance of a bidirectional horizontal-axis tidal turbine with passive flow control devices', *Renewable Energy*, 194, pp. 997–1008.